Nano Research
2019, 12(8): 1789–1795

ISSN 1998-0124 CN 11-5974/O4
https://doi.org/10.1007/s12274-019-2433-5

Research Article

A laser ablated graphene-based flexible self-powered pressure sensor for human gestures and finger pulse monitoring

Partha Sarati Das[§], Ashok Chhetry[§], Pukar Maharjan, M. Salauddin Rasel, and Jae Yeong Park (✉)

Micro/Nano Devices & Packaging Lab., Dept. of Electronic Engineering, Kwangwoon University, Seoul, 01897, Republic of Korea
[§]Partha Sarati Das and Ashok Chhetry contributed equally to this work.

Received: 25 January 2019 / **Revised:** 6 May 2019 / **Accepted:** 10 May 2019

ABSTRACT

Flexible triboelectric nanogenerators (TENGs)-based pressure sensors are very essential for the wide-range applications, comprising wearable healthcare systems, intuitive human-device interfaces, electronic-skin (e-skin), and artificial intelligence. Most of conventional fabrication methods used to produce high-performance TENGs involve plasma treatment, photolithography, printing, and electro-deposition. However, these fabrication techniques are expensive, multi-step, time-consuming and not suitable for mass production, which are the main barriers for efficient and cost-effective commercialization of TENGs. Here, we established a highly reliable scheme for the fabrication of a novel eco-friendly, low cost, and TENG-based pressure sensor (TEPS) designed for usage in self-powered-human gesture detection (SP-HGD) likewise wearable healthcare applications. The sensors with microstructured electrodes performed well with high sensitivity (7.697 kPa^{-1}), a lower limit of detection (~ 1 Pa), faster response time (< 9.9 ms), and highly stable over > 4,000 compression–releasing cycles. The proposed method is suitable for the adaptable fabrication of TEPS at an extremely low cost with possible applications in self-powered systems, especially e-skin and healthcare applications.

KEYWORDS

flexible, laser ablated graphene, self-powered, triboelectric nanogenerator, human gestures, finger pulse

1 Introduction

There is a developing interest in a large area, flexible, and stretchable e-skins for facilitating robots and wearable electronics. A vital application of e-skins is the seamless sensing of pressure in human interactions. Human skin contains various types of touch receptors that reply to various types and degrees of mechanical forces. Highly sensitive piezoelectric-type, resistive-type, and capacitive-type microstructured/nanostructured pressure sensors have been reported [1–9]. In recent years, an innovative kind of pressure sensing device known as a triboelectric nanogenerator (TENG) was established on a coupling mechanism between the "triboelectric-charge and electrostatic-induction" [10–13]. This novel TENG technology was first reported by Fan et al. in 2012 [14]. Owing to the numerous benefits of TENGs, for example, their low-cost, simple engineering procedure, and high-power-density, they can be implemented successfully as self-powered pressure sensors without requiring a storage cell or outer energy supply [15–17]. TENGs pressure sensor has many potential commercial applications in sensing devices [18–20]. However, the mass fabrication of these pressure-sensing devices utilizing non-conventional materials is still challenging [21–23]. TENG-based pressure sensor (TEPS) has a great possibility to be used as self-powered applications because of their simple structure and fabrication [24–26]. Most previously reported TEPSs have large sensitivity at low-pressures (< 1 kPa) to allow ultra-sensitive detection, however, the sensitivity declines notably at large-pressures, thereby making them unsuitable for real applications [27, 28]. For example, mild touching and object handling can produce pressures that are lower than 10 kPa and between 10 and 100 kPa, respectively. Thus, there is a high demand to sustain larger sensitivity within a broad-range pressure. One of the essential issues that affect the performance of the contact-electrification procedure is the surface structure of the triboelectric contact faces, which determines the charge generation procedure throughout contact electrification. Various approaches have been conceived to enhance the surface structure and properties, including soft lithography, plasma etching, nanoparticle deposition, block copolymer self-assembly, and chemical-treatment [29–31]. However, these fabrication methods and techniques are expensive and also inappropriate for fabricating relatively large samples. Hence, it is desirable to develop alternative methods for fabricating self-powered pressure sensors using low-cost techniques [32]. However, the adaptability and expenditure of the available fabrication methods still hinder the commercial production of the devices based on the triboelectric mechanism [33]. Moreover, the adaptability of the fabrication procedures is also vital for producing large-scale sensors. In order to measure pressure over large surfaces, it is required to make a large-scale sensor [34]. The application area such as artificial skin (e-skin), the tactile system for future robots, foot and gait pressure measurement and human activity recognition through pressure mapping all needs large-scale flexible sensor arrays [35]. For example, a sensor with a small area can cover few areas which make the data acquisition system complex and also, the fabrication of a sensor comprising of many pressure arrays is difficult in conventional fabrication techniques. The current TENG fabrication techniques have the limitations of wafer-size or chamber-size in the fabrication set-up, thereby restraining their suitability to small samples. To address these limitations, it is essential to develop inexpensive, large scale flexible sensors that are reliable, mechanically-robust, and electrically-

Address correspondence to jaepark@kw.ac.kr

stable with iterative external forces. Here, we created a self-powered triboelectric pressure sensor using laser ablated graphene (LAG) [36] and abrasive sandpaper [37], which was used to implement a pressure sensor with high sensitivities (7.697, 0.938 and 0.136 kPa^{-1}) over a large range (up to 100 kPa). The newly designed LAG-TEPS has dramatically improved mechanical flexibility, and also the proposed LAG-TEPS exhibited excellent stability above 4,000 cycles of iterative contact-separation tests. The proposed LAG-TEPS can be applied fruitfully in the human body and used in self-powered-human gesture detection (SP-HGD) processes for body-based wearable applications as well as healthcare applications [38]. The LAG and sandpaper fabrication processes facilitate the large sample, cheap, and time-saving production of reliable pressure sensors. An illustration of the proposed LAG-TEPS based on LAG and sandpaper is shown in Fig. 1(a).

The proposed LAG-TEPS mainly comprises three layers: A layer of microstructured polydimethylsiloxane (PDMS) with LAG attached to the bottom, which acts as the bottom electrode; and a polyethylene terephthalate/indium tin oxide (PET/ITO) film with opposite triboelectric polarity (Fig. S1 in the Electronic Supplementary Materials (ESM)), where the whole configuration is inserted in the middle of 2 acrylic sheets, as presented in Fig. 1(a). The main principle of the suggested LAG-TEPS is illustrated in Fig. 1(b). In the proposed LAG-TEPS, triboelectric charging happens at the contact surface interface due to iterative physical contact between the microstructured PDMS and ITO materials with dissimilar polarities with regard to the triboelectric series [39–41]. Initially, the surface charges are generated via the electrification effect and then a potential difference established by electrostatic induction. The triboelectric pair comprising the microstructured PDMS and ITO is isolated at the preliminary condition, so the LAG-TEPS is electrically impartial with no charges on the surface. The upper slice of the LAG-TEPS is pushed down to touch the bottom slice of the LAG-TEPS using an external force as shown in Fig. 1(b).

In addition, electrons are created at the surface between the microstructured PDMS and ITO films because of the electrification process. An inner electric potential is produced when the pressure is detached since the 2 slices of the LAG-TEPS are separated. While

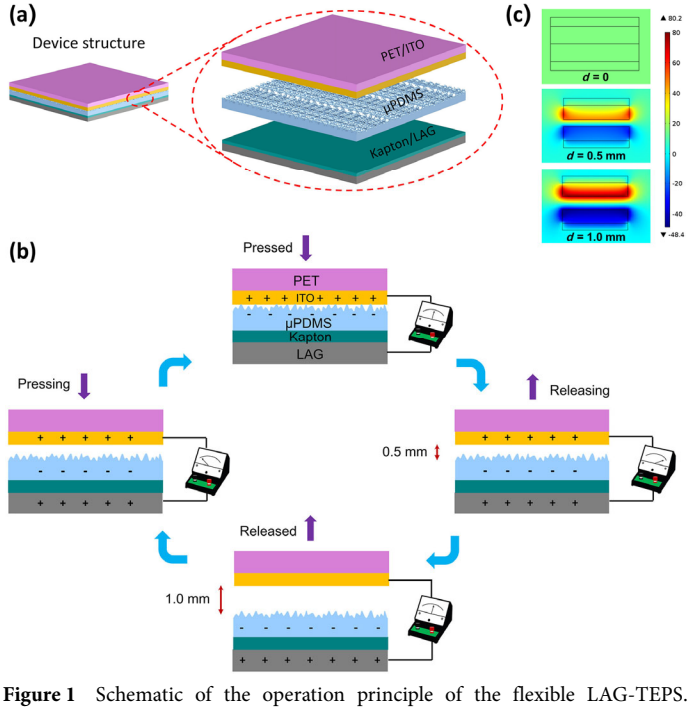

Figure 1 Schematic of the operation principle of the flexible LAG-TEPS. (a) Flexible LAG-TEPS and inset shows its structure. (b) Working principle of the LAG-TEPS. (c) Finite-element analysis (FEA) simulation of the generated voltage.

the distance between the two slices deviates, the inner potential drop varies, as a result, the total charge will be collected by ITO & LAG due to electrostatic field effect. Thus, the current flows in the closed-circuit loop when the electrodes on the LAG-TEPS are associated with the load. Likewise, the performance can be further developed by using a nanostructured PDMS-based LAG-TEPS. The proposed LAG-TEPS can be functioned in two modes based on the output voltage = V_{pp} and output current = I_{pp}.

Furthermore, to explain the working principle of our device, FEA technique, COMSOL Multiphysics software was utilized to examine the potential drop distribution in the proposed LAG-TEPS. We observed that the potential drop variation between the ITO and LAG decreased as the separation increased. We also estimated the V_{pp} in the LAG-TEPS based on distances of 0.5 and 1.0 mm, as indicated in the upper and lower portion of Fig. 1(c). The V_{pp} decreased as the distance increased because the electrification outcome was obtained by the gap separating the two opposing triboelectric materials throughout periodic contact-separation mode. To deliver a more comprehensive explanation, the separation distance and contact surface area were altered by pressing an external force, and the finite-element technique in COMSOL software was applied after measuring the amount of charge per unit region, where Eq. (1) was employed. The electric potential distribution was simulated in the open state in Fig. 1(c). The electric potential distribution of the V_{pp} is defined as follows [42]

$$V_{PP} = \frac{\sigma_{PDMS} \cdot d_0}{\varepsilon_0} \tag{1}$$

where σ_{PDMS} is the amount of charge per unit region, d_0 is the separation between the ITO and LAG electrodes, and ε_0 = free space permittivity. The charge density of ITO, PDMS, and LAG electrodes in the equilibrium state is defined as follows [43]

$$\sigma_{ITO} + \sigma_{PDMS} + \sigma_{LAG} = 0 \tag{2}$$

where the subscripts ITO, PDMS, and LAG represent indium tin oxide, polydimethylsiloxane, and laser ablated graphene, respectively. The potential difference between the ITO and LAG is achieved using an electric field (E-field) line integration, which might be said as follows

$$V_f = \int_0^{d_T+d} E \cdot \mathrm{d}l = \frac{\sigma_{ITO}}{2\varepsilon_0}\left(\frac{d_T}{\varepsilon_T} + d_0\right) + \frac{\sigma_{LAG}}{2\varepsilon_0}\left(\frac{d_T}{\varepsilon_T} + d_0\right) + \frac{\sigma_{PDMS}}{2\varepsilon_0}\left(-\frac{d_T}{\varepsilon_T} + d_0\right) = 0 \tag{3}$$

where ε_T is the relative dielectric permittivity of PDMS, d_T is the thickness of the PDMS sheet, d_0 is the distance between the LAG and the ITO electrode, and ε_0 is the free-space dielectric permittivity. If the electrical thickness of PDMS as $d_{TE} = d_T/\varepsilon_T$ and combining (2) and (3)

$$\sigma_{ITO} = -\sigma_{PDMS}\frac{1}{1 + d_{TE}/d_0} = 0, \text{ and } \sigma_{LAG} = -\sigma_{PDMS}\frac{1}{1 + d_0/d_{TE}} = 0 \tag{4}$$

The average of output current, I_{pp}, flowing from the ITO to the LAG can be related as

$$I_{pp} = \frac{\Delta Q}{\Delta t} = \frac{A(\sigma_{ITO}^f - \sigma_{ITO}^i)}{\Delta t} = \frac{\Delta \tau_{PDMS}}{\Delta t}\left(\frac{d_i}{d_i + d_{TE}} - \frac{d_f}{d_i + d_{TE}}\right) \tag{5}$$

where the preliminary and ending distances between the ITO and LAG are d_i and d_f, A is surface areas, and Δt is movement in seconds. According to Eqs. (4) and (5), when the ITO and the PDMS sheet are close to each other (which means $d_f < d_i$), then the current is negative. But when the ITO is moved ($d_f > d_i$), the positive current

flows in the reverse direction. When the ITO and LAG are in without load, their electric potential difference is able to vary with space d_0. The potential difference is zero at an initial stage but it can be defined at the final state as below

$$V_{PP} = \int_0^{d_T+d} E \cdot dl = \frac{\sigma_{LAG} - \sigma_{ITO}}{2\varepsilon_0}(d_{TE} + d_f) - \frac{\sigma_{PDMS}}{2\varepsilon_0}(d_{TE} - d_0) \quad (6)$$

From Eqs. (6) and (4)

$$V_{PP} = \frac{\sigma_{PDMS}}{\varepsilon_0} \cdot \frac{\sigma_{TE}(d_i - d_f)}{d_i + d_{TE}} \quad (7)$$

when the ITO moves down to make contact with the PDMS, if d_f = 0, the voltage between the plates reaches [65]

$$V_{PP} = \frac{\sigma_{PDMS}}{\varepsilon_0} \cdot \frac{\sigma_{TE} \cdot \tau_i}{d_i + d_{TE}} \quad (8)$$

2 Experimental

2.1 Fabrication of microstructured electrodes

To make the PDMS microstructures, a piece of sandpaper was tape-fixed on the upper side of a silicon wafer as presented in Fig. 2 (a) [44]. We made a solution of PDMS elastomer with its crosslinker (SYLGARD® 184, Dow Corning) mixed at 10:1 weight ratio and then steadily poured on sandpaper. Next, it was spin coated (SCS 6800, Specialty Coating System) on the sandpaper for 35 s. In order to remove the bubble from the spin-coated solution, we performed

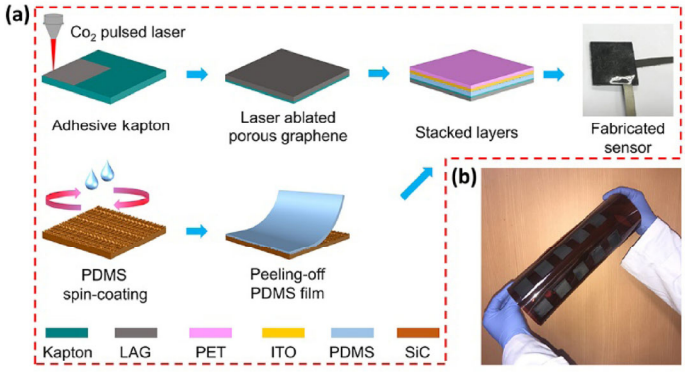

Figure 2 (a) Illustration of the fabrication sequence for the proposed TENG. Laser-ablated porous graphene on microstructured PDMS and PET/ITO were assembled together to make flexible LAG-TEPS. (b) Photograph of the LAG illustrating the scalable fabrication.

20 min of degasification in a vacuum. Then the solution was cured at 80 °C for 1 h. Finally, a thin (200 μm) microstructured PDMS film was peeled off from sandpaper template.

2.2 LAG fabrication

As depicted in Fig. 2(a), the LAG was fabricated by one-step laser scribing on a thin and highly flexible adhesive Kapton® polyimide (PI, 55 μm) film. The PI substrate was cleaned separately by isopropyl alcohol (IPA), methanol, and deionized (DI) water. Then, a CO_2 pulsed laser (15 W) was used to convert the PI film into porous graphene under ambient conditions [45–47].

2.3 Fabrication of the LAG-TEPS

A stack-like architecture was employed for the design of the LAG-TEPS as shown in Fig. 1(a). We attached the opposite layer of the rough PDMS surface to the adhesive side of the LAG. We used 127 μm thick commercial PET/ITO film as the friction material. The PET/ITO film was adhered to the surface of the microstructured PDMS layer. The total area of the LAG-TEPS was 12 cm^2 as shown in Fig. 1(a). An image of fabricated large-scaled LAG sample is illustrated in Fig. 2(b). The total 25 samples with unit sample size of 3 cm × 3 cm was prepared.

2.4 Electrical and physical characterization

Figure 3(a) shows the image of the LAG on Kapton and the inset illustrates the FE-SEM image of the corresponding LAG. The sheet resistance of the LAG and PET/ITO films were 40 Ω/sq. and 100 Ω/sq., respectively. The sheet resistivity meter (RC2175, EDTM) [48] was used to measure the sheet resistance, as shown in Figs. 3(b) and 3(c), respectively. The roughness of the PDMS surface was characterized by FE-SEM (FEI, Quanta 250 FEG), as shown in Fig. 3(d), where the microstructures are clearly seen on the PDMS surface. One of the crucial factors responsible for increasing the contact area is the surface roughness that essentially changes the effective rubbing area owing to the surface pattern. Thus, increasing the surface irregularity enhances the electrical properties of a LAG-TEPS. Hence, we employed a stamping procedure based on sandpaper to produce the microstructure on the surface of the PDMS layer. The non-uniform microstructure on the surface of the sandpaper was simply transferred into the surface of the PDMS, bringing greater sensitivity under high pressures. The electrical performance of the LAG-TEPS was measured using a digital oscilloscope (WaveSurfer 510 Oscilloscope, Teledyne LeCroy), Datalogger (DrDAQ) and an electrometer (Keithley 6514) to measure the V_{PP} and I_{PP}. The sensitivity was measured and characterized using a model comprising JSV-H1000 and HF-10, JISC. The characterizations and investigations of the LAG-TEPS were

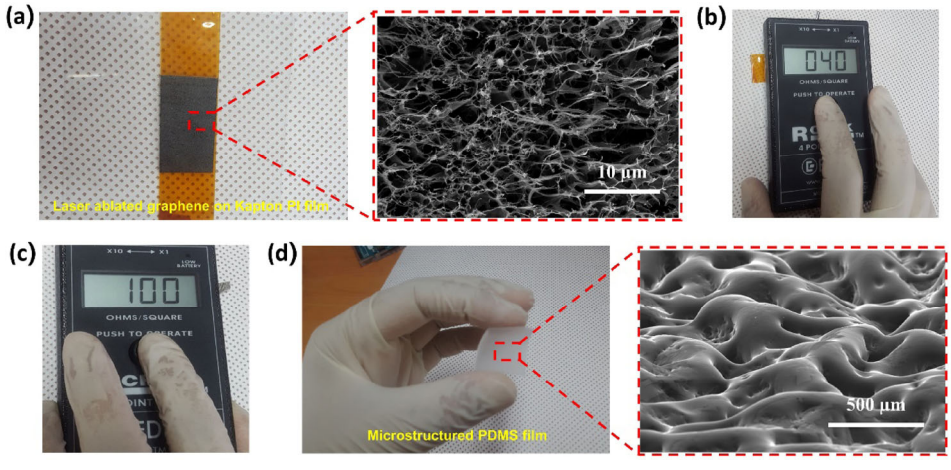

Figure 3 Physical & electrical characterization of flexible LAG-TEPS. (a) Field emission scanning electron microscopy (FE-SEM) image of LAG. (b) Sheet resistance of LAG. (c) Sheet resistance of PET/ITO. (d) FESEM image of microstructured PDMS.

obtained under ambient circumstances at a temperature and humidity of 25 °C, 30%–35%.

3 Results and discussion

3.1 Pressure sensor response

The proposed LAG-TEPS is composed of two frictional layers: a microstructured PDMS film as one frictional material and the ITO-coated PET, which served as the opposite frictional component. The operation principle of the pressure sensor can be classified as a single electrode mode TENG according to the four kinds of fundamental modes of TENG. When the triboelectric materials come in contact with each other, identical amounts of triboelectric positive and negative charges formed over the surfaces of the microstructured PDMS and ITO owing to their dissimilar triboelectric polarities. Two equally sized acrylic sheets were utilized to examine the response of the LAG-TEPS to dynamic loadings. Figures 4(a) and 4(b) show the V_{pp} and I_{pp} of the TENG at a frequency of 4 Hz, respectively. The average V_{pp} and I_{pp} values reached about ~ 60 V and ~ 14 nA, respectively. The output voltage has bidirectional peaks because positive and negative peaks come from pressing and releasing condition from Fig. 1(b). Additional peaks come due to the inertia of static charge which is shown in the inset of Fig. 4(a). The V_{pp} and I_{pp} of the LAG-TEPS under external load are shown in Fig. S2 in the ESM. Furthermore, the LAG-TEPS exhibited good stability under a mechanical pressure of 30 kPa at a frequency of 0.5 Hz for 4,000 cycles with no significant degradation in the performance, as illustrated in Fig. 4(c). The average value of I_{pp} was about 50 nA. The dynamic pressure loading was used to investigate the response of the LAG-TEPS. The LAG-TEPS electrical output profiles were analyzed to calculate the sensitivity from the resulting electric signals with respect to change in the applied pressures.

The V_{pp} produced by a TENG relies on the σ, which is influenced by the surface contact area between two different polymers. We found that as the mechanical pressure increased gradually, the surface contact region increased caused by macroscopic change at the interface across the two dissimilar polymers, as shown in Figs. 4(d) and 4(e), respectively. When the two dissimilar polymers get in touch with each other, the electrification induced surface charges get saturated, thereby preventing any additional enhancement in the V_{pp}, as shown in Fig. 4(f). The sensitivity can be expressed as [3]

$$S = \frac{\left(\Delta I_{pp}/I_{opp}\right)}{\Delta P} \tag{9}$$

$$\Delta I_{pp} = I_{pp} - I_{opp} \tag{10}$$

where I_{opp} is the output current without pressure, ΔI_{pp} is the calculated output current change when an outer pressure is applied, and ΔP is the change in pressure. The response time of the LAG-TEPS was excellent with a rise time of only 9.9 ms, which we calculated based on the enlarged output current signal, as shown in Fig. 5(a). The external pressure with respect to the displacement behavior of LAG-TEPS for loading and unloading cycle is shown in Fig. S3 in the ESM. The sensor exhibited three distinct sensitivity values up to 100 kPa. The sensitivities of the pressure sensor in the low-pressure region (< 1 kPa), medium-pressure region (1–20 kPa), and high-pressure region (> 20 kPa) were 7.697, 0.938, and 0.136 kPa^{-1},

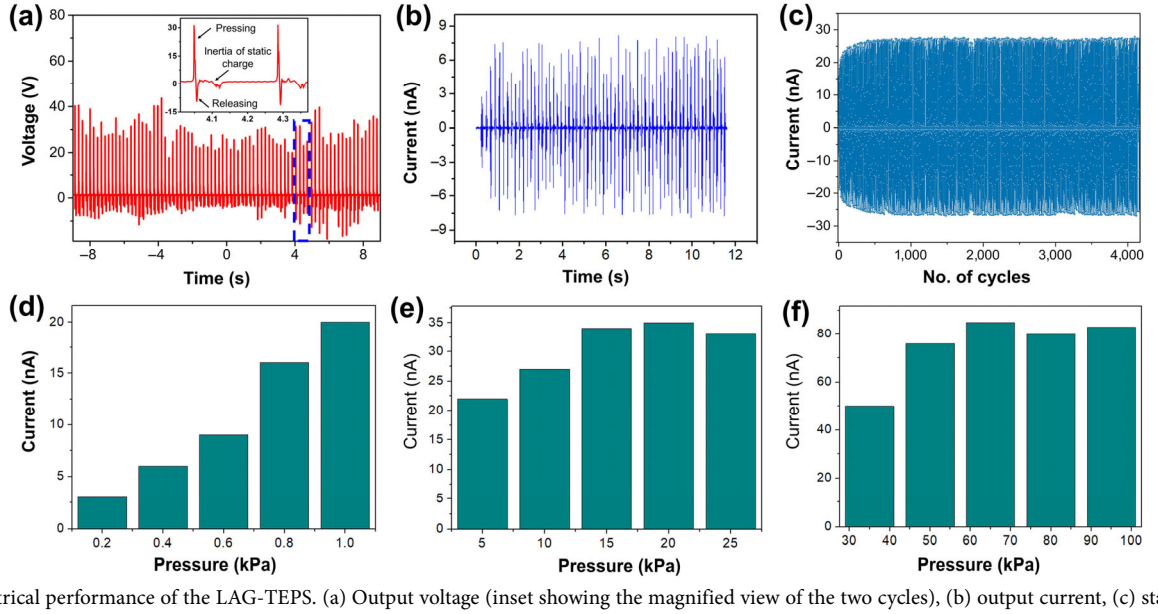

Figure 4 Electrical performance of the LAG-TEPS. (a) Output voltage (inset showing the magnified view of the two cycles), (b) output current, (c) stability test over > 4,000 cycles. Output current (d) under low pressure, (e) in the medium pressure, and (f) in the high-pressure region.

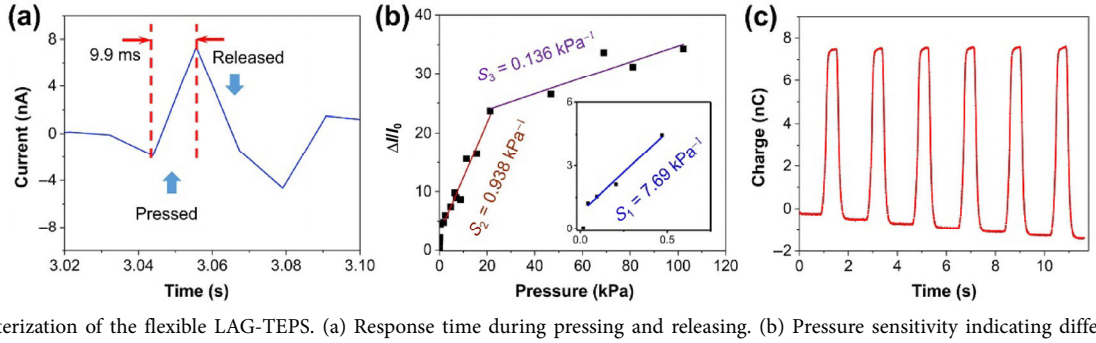

Figure 5 Characterization of the flexible LAG-TEPS. (a) Response time during pressing and releasing. (b) Pressure sensitivity indicating different sensitivities at different pressure regimes. (c) Transferred charges of LAG-TEPS.

respectively. The sensitivity was estimated based on the current response slope, as shown in Fig. 5(b). An enlarged view of the sensitivity in the low-pressure region from 0 to 1 kPa is shown in the inset of Fig. 5(b). The LAG-TEPS revealed high sensitivity within low to medium (< 1–20 kPa) pressure ranges. On the other hand, the sensitivity of the LAG-TEPS declined to 0.136 kPa^{-1} for pressure above 70 kPa, which is because of the output current saturated when the pressure increased. At low (0–1 kPa) and medium (1–20 kPa) pressures, the pressure sensor exhibited a linear enlargement in the output current as the dynamic pressure increased, as shown in Fig. 5(b). The quantity of transferred charge reached 7.5 nC under a mechanical pressure of 1 kPa with rising time of 0.35 and 0.47 s as presented in Fig. 5(c). The experimental setup for the electro-mechanical analysis of the as-fabricated LAG-TEPS is depicted in Fig. S4 in the ESM. Table 1 shows the performance comparison of our sensor with recently reported pressure sensors. The enhanced pressure sensitivity of 7.697 kPa^{-1} was achieved, which is better than many recently reported pressure sensors. The LAG-TEPS showed excellent sensitivity both in the low-pressure and medium-pressure region with a wider working range.

3.2 Self-powered human gestures detection

Our LAG-TEPS designed with flexibility and high sensitivity is particularly suitable for e-skin applications because of its flexible and highly sensitive nature to externally applied pressures [49–57]. We investigated the flexibility of the pressure sensor in terms of its action as an SP-HGD. To examine the performance of the pressure sensor for sensing human gestures, LAG-TEPS was finger tapped and attached to the different portions of the human body, for example, the elbow, knee, and wrist as shown in photograph image of Fig. 6(a).

For the illustration of LAG-TEPS in an e-skin application, we pressed the LAG-TEPS using a finger tapping and the electric signal from the LAG-TEPS changed immediately, as shown in Fig. 6(b) (Video ESM1-Finger tapping). The self-powered signals obtained throughout iterative bending-stretching cycles are displayed in Figs. 6(c)–6(e) (Video ESM2-Small vibration and Video ESM3-Human gestures). The pressure sensor revealed great responsiveness and stable repeatability under gestures owing to body movements, and without requiring a storage cell or outer energy supply. Different signal shapes were produced using LAG-TEPS sensor to distinguish various human body gestures, including the finger, knee, and elbow. These outcomes demonstrate that the LAG-TEPS might be utilized in wearable sensors due to its ability for SP-HGD.

3.3 Finger pulse monitoring

The high sensitivity and rapid response time of pressure sensors are advantageous for uses in bio-health monitoring and telemedicine. For example, the sensor can be put over the human skin for pulse and blood pressure if correctly calibrated. In this study, we also investigated and demonstrated that our LAG-TEPS can be used for detecting the pulse from the human fingertips as reported in [58], even though it was operated through the power supply. Figure 6(f) shows the signal obtained from the proposed LAG-TEPS system when a human finger was put over the sensor. The sensor output from the human fingertip exhibited a clear pulse waveform. The finger

Table 1 Performance comparison of recently developed pressure sensors

Type	Materials	Pressure range (kPa)	Sensitivity (kPa^{-1})	Ref.
Resistive	rGO coated sponge	< 2/2–10	0.26/0.03	[59]
Resistive	CB coated sponge	0.091/16.4	0.068/0.023	[60]
Piezoelectric	PDMS-Gold-(P(VDF-TrFE))	< 5/60–600	0.104/0.055	[61]
Piezoresistive	Graphene-PDMS	< 0.25/1–8	–0.24/0.034	[62]
Capacitive	SWNT-PDMS-Ecoflex	10–200	0.59	[63]
Triboelectric	PVDF-AgNPs	< 40/40–160	0.385/0.065	[64]
Triboelectric	LAG-μPDMS-ITO/PET	< 1/1–20	7.697/0.938	This work

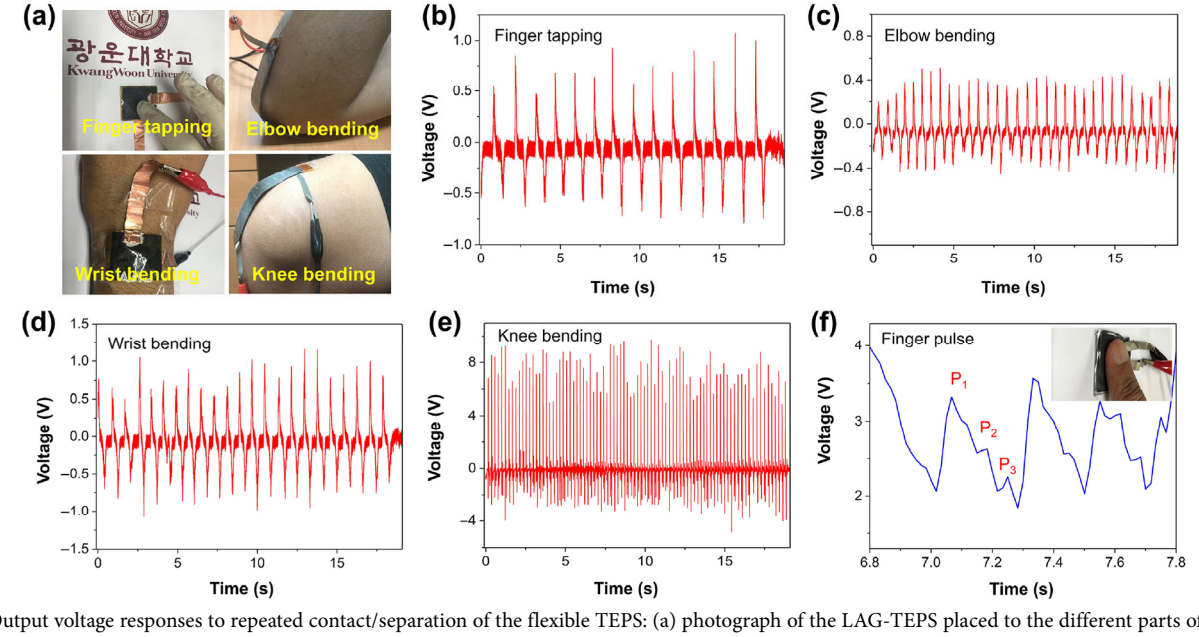

Figure 6 Output voltage responses to repeated contact/separation of the flexible TEPS: (a) photograph of the LAG-TEPS placed to the different parts of the body for the detection of human gestures. The corresponding voltage response for (b) finger tapping, (c) elbow bending, (d) wrist bending, (e) knee bending, and (f) finger pulses.

pulse signal was sorted out by a resistor-capacitor bandpass filter and digital converter (ADC, Arduino UNO) after the instrumentation amplification (AD624). Finally, we used MATLAB to eliminate the noise from the obtained signal using a finite impulse response (FIR) filter. The Arduino UNO output was visualized on a computer using open source demonstration processing software (sampling rate: 1 kHz, 2-bit resolution) [65]. Videos of self-powered human gestures detection can be found in the ESM.

4 Conclusion

In summary, we fabricated and analyzed a LAG-TEPS established on the triboelectric principle to implement self-powered sensing without an outer storage cell. The response time and the sensitivity of the LAG-TEPS were 9.9 ms and 7.697 kPa^{-1}, respectively. Moreover, LAG-TEPS was put to several parts of the body, and we showed that based on the mechanical deformation due to iterative human gestures, it was promising to operate the device in a stable manner via upward and downward directions. Therefore, this LAG-TEPS sensor can be self-powered and it does not require an outer power source. We also demonstrated that our LAG-TEPS can be applied as a pulse monitoring sensor with an outer power supply. Our proposed method can potentially facilitate the large-scale production of flexible, self-powered, and inexpensive pressure sensors in a time-efficient manner.

Acknowledgements

This research was supported by the Bio & Medical Technology Development Program of the NRF grant funded by the Korean government (MSIT) (No. NRF-2017M3A9F1031270).

Electronic Supplementary Material: Supplementary material (further details of the triboelectric series, current/voltage variations, stress-strain behavior, and experimental setup) is available in the online version of this article at https://doi.org/10.1007/s12274-019-2433-5.

References

[1] Xia, K. L.; Wang, C. Y.; Jian, M. Q.; Wang, Q.; Zhang, Y. Y. CVD growth of fingerprint-like patterned 3D graphene film for an ultrasensitive pressure sensor. *Nano Res*. **2018**, *11*, 1124–1134.

[2] Someya, T.; Sekitani, T.; Iba, S.; Kato, Y.; Kawaguchi, H.; Sakurai, T. A large-area, flexible pressure sensor matrix with organic field-effect transistors for artificial skin applications. *Proc. Natl. Acad. Sci. USA* **2004**, *101*, 9966–9970.

[3] Liu, Y.; Tao, L. Q.; Wang, D. Y.; Zhang, T. Y.; Yang, Y.; Ren, T. L. Flexible, highly sensitive pressure sensor with a wide range based on graphene-silk network structure. *Appl. Phys. Lett*. **2017**, *110*, 123508.

[4] Chhetry, A.; Yoon, H.; Park, J. Y. A flexible and highly sensitive capacitive pressure sensor based on conductive fibers with a microporous dielectric for wearable electronics. *J. Mater. Chem. C* **2017**, *5*, 10068–10076.

[5] Park, S. W.; Das, P. S; Park, J. Y. Development of wearable and flexible insole type capacitive pressure sensor for continuous gait signal analysis. *Org. Electron*. **2018**, *53*, 213–220.

[6] Maiolino, P.; Maggiali, M.; Cannata, G.; Metta, G.; Natale, L. A flexible and robust large scale capacitive tactile system for robots. *IEEE Sens. J*. **2013**, *13*, 3910–3917.

[7] Fuh, Y. K.; Wang, B. S.; Tsai, C. Y. Self-powered pressure sensor with fully encapsulated 3D printed wavy substrate and highly-aligned piezoelectric fibers array. *Sci. Rep*. **2017**, *7*, 6759.

[8] Tian, H.; Shu, Y.; Wang, X. F.; Mohammad, M. A.; Bie, Z.; Xie, Q. Y.; Li, C.; Mi, W. T.; Yang, Y.; Ren, T. L. A graphene-based resistive pressure sensor with record-high sensitivity in a wide pressure range. *Sci. Rep*. **2015**, *5*, 8603.

[9] Park, S. W.; Das, P. S.; Chhetry, A.; Park, J. Y. A flexible capacitive pressure sensor for wearable respiration monitoring system. *IEEE Sens. J*. **2017**, *17*, 6558–6564.

[10] Mao, Y. C.; Geng, D. L.; Liang, E. J.; Wang, X. D. Single-electrode triboelectric nanogenerator for scavenging friction energy from rolling tires. *Nano Energy* **2015**, *15*, 227–234.

[11] Sun, J. G.; Yang, T. N.; Kuo, I. S.; Wu, J. M.; Wang, C. Y.; Chen, L. J. A leaf-molded transparent triboelectric nanogenerator for smart multifunctional applications. *Nano Energy* **2017**, *32*, 180–186.

[12] Dudem, B.; Kim, D. H.; Yu, J. S. Triboelectric nanogenerators with gold-thin-film-coated conductive textile as floating electrode for scavenging wind energy. *Nano Res*. **2018**, *11*, 101–113.

[13] Mallineni, S. S. K.; Dong, Y. C.; Behlow, H.; Rao, A. M.; Podila, R. A wireless triboelectric nanogenerator. *Adv. Energy Mater*. **2018**, *8*, 1702736.

[14] Fan, F. R.; Tian, Z. Q; Wang, Z. L. Flexible triboelectric generator. *Nano Energy* **2012**, *1*, 328–334.

[15] Zhu, G.; Yang, W. Q.; Zhang, T. J.; Jing, Q. S.; Chen, J.; Zhou, Y. S.; Bai, P.; Wang, Z. L. Self-powered, ultrasensitive, flexible tactile sensors based on contact electrification. *Nano Lett*. **2014**, *14*, 3208–3213.

[16] Yi, F.; Lin, L.; Niu, S. M.; Yang, P. K.; Wang, Z. N.; Chen, J.; Zhou, Y. S.; Zi, Y. L.; Wang, J.; Liao, Q. L. et al. Stretchable-rubber-based triboelectric nanogenerator and its application as self-powered body motion sensors. *Adv. Funct. Mater*. **2015**, *25*, 3688–3696.

[17] Niu, S. M.; Wang, Z. L. Theoretical systems of triboelectric nanogenerators. *Nano Energy* **2015**, *14*, 161–192.

[18] Lee, K. Y.; Yoon, H. J.; Jiang, T.; Wen, X. N.; Seung, W.; Kim, S. W.; Wang, Z. L. Fully packaged self-powered triboelectric pressure sensor using hemispheres-array. *Adv. Energy Mater*. **2016**, *6*, 1502566.

[19] Lim, G. H.; Kwak, S. S.; Kwon, N.; Kim, T.; Kim, H.; Kim, S. M.; Kim, S. W.; Lim, B. Fully stretchable and highly durable triboelectric nanogenerators based on gold-nanosheet electrodes for self-powered human-motion detection. *Nano Energy* **2017**, *42*, 300–306.

[20] Cai, F.; Yi, C. R.; Liu, S. C.; Wang, Y.; Liu, L. C.; Liu, X. Q.; Xu, X. M.; Wang, L. Ultrasensitive, passive and wearable sensors for monitoring human muscle motion and physiological signals. *Biosens. Bioelectron*. **2016**, *77*, 907–913.

[21] Zhang, L.; Jin, L.; Zhang, B. B.; Deng, W. L.; Pan, H.; Tang, J. F.; Zhu, M. H.; Yang, W. Q. Multifunctional triboelectric nanogenerator based on porous micro-nickel foam to harvest mechanical energy. *Nano Energy* **2015**, *16*, 516–523.

[22] Pan, L.; Wang, J. Y.; Wang, P. H.; Gao, R. J.; Wang, Y. C.; Zhang, X. W.; Zou, J. J.; Wang, Z. L. Liquid-FEP-based U-tube triboelectric nanogenerator for harvesting water-wave energy. *Nano Res*. **2018**, *11*, 4062–4073.

[23] Yang, P. K.; Lin, L.; Yi, F.; Li, X. H.; Pradel, K. C.; Zi, Y. L.; Wu, C. I.; He, J. H.; Zhang, Y.; Wang, Z. L. A flexible, stretchable and shape-adaptive approach for versatile energy conversion and self-powered biomedical monitoring. *Adv. Mater*. **2015**, *27*, 3817–3824.

[24] Luo, J. J.; Fan, F. R.; Jiang, T.; Wang, Z. W.; Tang, W.; Zhang, C. P.; Liu, M. M.; Cao, G. Z.; Wang, Z. L. Integration of micro-supercapacitors with triboelectric nanogenerators for a flexible self-charging power unit. *Nano Res*. **2015**, *8*, 3934–3943.

[25] Dhakar, L.; Pitchappa, P.; Tay, F. E. H.; Lee, C. An intelligent skin based self-powered finger motion sensor integrated with triboelectric nanogenerator. *Nano Energy* **2016**, *19*, 532–540.

[26] Garcia, C.; Trendafilova, I.; De Villoria, R. G.; Del Rio, J. S. Self-powered pressure sensor based on the triboelectric effect and its analysis using dynamic mechanical analysis. *Nano Energy* **2018**, *50*, 401–409.

[27] Hwang, B. U.; Lee, J. H.; Trung, T. Q.; Roh, E.; Kim, D. I.; Kim, S. W.; Lee, N. E. Transparent stretchable self-powered patchable sensor platform with ultrasensitive recognition of human activities. *ACS Nano* **2015**, *9*, 8801–8810.

[28] Yu, L. H.; Yi, Y. Y.; Yao, T.; Song, Y. Z.; Chen, Y. R.; Li, Q. C.; Xia, Z.; Wei, N.; Tian, Z. N.; Nie, B. Q. et al. All VN-graphene architecture derived self-powered wearable sensors for ultrasensitive health monitoring. *Nano Res*. **2019**, *12*, 331–338.

[29] Choi, A. Y.; Lee, C. J.; Park, J.; Kim, D.; Kim, Y. T. Corrugated textile based triboelectric generator for wearable energy harvesting. *Sci. Rep*. **2017**, *7*, 45583.

[30] Das, P. S.; Park, J. Y.; Kim, D. H. Vacuum filtered conductive nylon membrane-based flexible TENG for wearable electronics. *Micro Nano Lett*. **2017**, *12*, 697–700.

[31] Das, P. S.; Park, J. Y. Human skin based flexible triboelectric nanogenerator using conductive elastomer and fabric films. *Electron. Lett*. **2016**, *52*, 1885–1887.

[32] Fan, F. R.; Lin, L.; Zhu, G.; Wu, W. Z.; Zhang, R.; Wang, Z. L. Transparent triboelectric nanogenerators and self-powered pressure sensors based on micropatterned plastic films. *Nano Lett*. **2012**, *12*, 3109–3114.
[33] Ma, M. Y.; Zhang, Z.; Liao, Q. L.; Yi, F.; Han, L. H.; Zhang, G. J.; Liu, S.; Liao, X. Q.; Zhang, Y. Self-powered artificial electronic skin for high-resolution pressure sensing. *Nano Energy* **2017**, *32*, 389–396.
[34] Cheng, J. Y.; Sundholm, M.; Zhou, B.; Hirsch, M.; Lukowicz, P. Smart-surface: Large scale textile pressure sensors arrays for activity recognition. *Pervasive Mob. Comput*. **2016**, *30*, 97–112.
[35] Ai, Y. F.; Hsu, T. H.; Wu, D. C.; Lee, L.; Chen, J. H.; Chen, Y. Z.; Wu, S. C.; Wu, C.; Wang, Z. M.; Chueh, Y. L. An ultrasensitive flexible pressure sensor for multimodal wearable electronic skins based on large-scale polystyrene ball@reduced graphene-oxide core–shell nanoparticles. *J. Mater. Chem. C* **2018**, *6*, 5514–5520.
[36] Dhakar, L.; Gudla, S.; Shan, X. C.; Wang, Z. P.; Tay, F. E. H.; Heng, C. H.; Lee, C. Large scale triboelectric nanogenerator and self-powered pressure sensor array using low cost roll-to-roll UV embossing. *Sci. Rep*. **2016**, *6*, 22253.
[37] Rasel, M. S.; Maharjan, P.; Salauddin, M.; Rahman, M. T.; Cho, H. O.; Kim, J. W.; Park, J. Y. An impedance tunable and highly efficient triboelectric nanogenerator for large-scale, ultra-sensitive pressure sensing applications. *Nano Energy* **2018**, *49*, 603–613.
[38] Li, Y. Q.; Huang, P.; Zhu, W. B.; Fu, S. Y.; Hu, N.; Liao, K. Flexible wire-shaped strain sensor from cotton thread for human health and motion detection. *Sci. Rep*. **2017**, *7*, 45013.
[39] Lee, C. J.; Choi, A. Y.; Choi, C.; Sim, H. J.; Kim, S. J.; Kim, Y. T. Triboelectric generator for wearable devices fabricated using a casting method. *RSC Adv*. **2016**, *6*, 10094–10098.
[40] Cui, S. W.; Zheng, Y. B.; Liang, J.; Wang, D. A. Triboelectrification based on double-layered polyaniline nanofibers for self-powered cathodic protection driven by wind. *Nano Res*. **2018**, *11*, 1873–1882.
[41] Jin, L. M.; Tao, J.; Bao, R. R.; Sun, L.; Pan, C. F. Self-powered real-time movement monitoring sensor using triboelectric nanogenerator technology. *Sci. Rep*. **2017**, *7*, 10521.
[42] Pu, X.; Liu, M. M.; Chen, X. Y.; Sun, J. M.; Du, C. H.; Zhang, Y.; Zhai, J. Y.; Hu, W. G.; Wang, Z. L. Ultrastretchable, transparent triboelectric nanogenerator as electronic skin for biomechanical energy harvesting and tactile sensing. *Sci. Adv*. **2017**, *3*, e1700015.
[43] Karagozler, M. E.; Poupyrev, I; Fedder, G. K.; Suzuki, Y. Paper generators: Harvesting energy from touching, rubbing and sliding. In *Proceedings of the 26th Annual ACM Symposium on User Interface Software and Technology*, St. Andrews, Scotland, UK, 2013, pp 23–30.
[44] Rasel, M. S. U.; Park, J. Y. A sandpaper assisted micro-structured polydimethylsiloxane fabrication for human skin based triboelectric energy harvesting application. *Appl. Energy* **2017**, *206*, 150–158.
[45] Lamberti, A.; Clerici, F.; Fontana, M.; Scaltrito, L. A highly stretchable supercapacitor using laser-induced graphene electrodes onto elastomeric substrate. *Adv. Energy Mater*. **2016**, *6*, 1600050.
[46] Lin, S. Y.; Feng, W. D.; Miao, X. F.; Zhang, X. X.; Chen, S. J.; Chen, Y. Q.; Wang, W.; Zhang, Y. N. A flexible and highly sensitive nonenzymatic glucose sensor based on DVD-laser scribed graphene substrate. *Biosens. Bioelectron*. **2018**, *110*, 89–96.
[47] Lin, J.; Peng, Z. W.; Liu, Y. Y.; Ruiz-Zepeda, F.; Ye, R. Q.; Samuel, E. L. G.; Yacaman, M. J.; Yakobson, B. I.; Tour, J. M. Laser-induced porous graphene films from commercial polymers. *Nat. Commun*. **2014**, *5*, 5714.
[48] R-CHEK surface resistivity meters [Online]. https://www.edtm.com/images/stories/pdf/manuals/r-chek_manual.pdf. (accessed Feb 4, 2019).
[49] Lee, S.; Reuveny, A.; Reeder, J.; Lee, S.; Jin, H.; Liu, Q. H.; Yokota, T.; Sekitani, T.; Isoyama, T.; Abe, Y. et al. A transparent bending-insensitive pressure sensor. *Nat. Nanotechnol*. **2016**, *11*, 472–478.
[50] Gong, S.; Schwalb, W.; Wang, Y. W.; Chen, Y.; Tang, Y.; Si, J.; Shirinzadeh, B.; Cheng, W. L. A wearable and highly sensitive pressure sensor with ultrathin gold nanowires. *Nat. Commun*. **2014**, *5*, 3132.
[51] Huang, Z. L.; Gao, M.; Yan, Z. C.; Pan, T. S.; Khan, S. A.; Zhang, Y.; Zhang, H. L.; Lin, Y. Pyramid microstructure with single walled carbon nanotubes for flexible and transparent micro-pressure sensor with ultra-high sensitivity. *Sens. Actuators A: Phys*. **2017**, *266*, 345–351.
[52] Kwak, Y. H.; Kim, W.; Park, K. B.; Kim, K.; Seo, S. Flexible heartbeat sensor for wearable device. *Biosens. Bioelectron*. **2017**, *94*, 250–255.
[53] Lipomi, D. J.; Vosgueritchian, M.; Tee, B. C. K.; Hellstrom, S. L.; Lee, J. A.; Fox, C. H.; Bao, Z. N. Skin-like pressure and strain sensors based on transparent elastic films of carbon nanotubes. *Nat. Nanotechnol*. **2011**, *6*, 788–792.
[54] Zhou, C. J.; Yang, Y. Q.; Sun, N.; Wen, Z.; Cheng, P.; Xie, X. K.; Shao, H. Y.; Shen, Q. Q.; Chen, X. P.; Liu, Y. N. et al. Flexible self-charging power units for portable electronics based on folded carbon paper. *Nano Res*. **2018**, *11*, 4313–4322.
[55] Wang, F.; Liu, S.; Shu, L.; Tao, X. M. Low-dimensional carbon based sensors and sensing network for wearable health and environmental monitoring. *Carbon* **2017**, *121*, 353–367.
[56] Xuan, X.; Kim, J. Y.; Hui, X.; Das, P. S.; Yoon, H. S.; Park, J. Y. A highly stretchable and conductive 3D porous graphene metal nanocomposite based electrochemical-physiological hybrid biosensor. *Biosens. Bioelectron*. **2018**, *120*, 160–167.
[57] Pang, Y.; Jian, J. M.; Tu, T.; Yang, Z.; Ling, J.; Li, Y. X.; Wang, X. F.; Qiao, Y. C.; Tian, H.; Yang, Y. et al. Wearable humidity sensor based on porous graphene network for respiration monitoring. *Biosens. Bioelectron*. **2018**, *116*, 123–129.
[58] Tee, B. C. K.; Chortos, A.; Dunn, R. R.; Schwartz, G.; Eason, E.; Bao, Z. N. Tunable flexible pressure sensors using microstructured elastomer geometries for intuitive electronics. *Adv. Funct. Mater*. **2014**, *24*, 5427–5434.
[59] Yao, H. B.; Ge, J.; Wang, C. F.; Wang, X.; Hu, W.; Zheng, Z. J.; Ni, Y.; Yu, S. H. A flexible and highly pressure-sensitive graphene–polyurethane sponge based on fractured microstructure design. *Adv. Mater*. **2013**, *25*, 6692–6698.
[60] Wu, X. D.; Han, Y. Y.; Zhang, X. X.; Zhou, Z. H.; Lu, C. H. Large-area compliant, low-cost, and versatile pressure-sensing platform based on microcrack-designed carbon black@polyurethane sponge for human–machine interfacing. *Adv. Funct. Mater*. **2016**, *26*, 6246–6256.
[61] Parida, K.; Bhavanasi, V.; Kumar, V.; Bendi, R.; Lee, P. S. Self-powered pressure sensor for ultra-wide range pressure detection. *Nano Res*. **2017**, *10*, 3557–3570.
[62] Chun, S.; Kim, Y.; Oh, H. S.; Bae, G.; Park, W. A highly sensitive pressure sensor using a double-layered graphene structure for tactile sensing. *Nanoscale* **2015**, *7*, 11652–11659.
[63] Wang, X. L.; Li, T. J.; Adams, J.; Yang, J. Transparent, stretchable, carbon-nanotube-inlaid conductors enabled by standard replication technology for capacitive pressure, strain and touch sensors. *J. Mater. Chem. A* **2013**, *1*, 3580–3586.
[64] Cao, R.; Wang, J. N.; Zhao, S. Y.; Yang, W.; Yuan, Z. Q.; Yin, Y. Y.; Du, X. Y.; Li, N. W.; Zhang, X. L.; Li, X. Y. et al. Self-powered nanofiber-based screen-print triboelectric sensors for respiratory monitoring. *Nano Res*. **2018**, *11*, 3771–3779.
[65] Signal display processing [Online]. https://processing.org/download/ (accessed Feb 3, 2019).